HHS Public Access

Author manuscript

NMR Biomed. Author manuscript; available in PMC 2017 January 01.

Published in final edited form as:

NMR Biomed. 2016 January ; 29(1): 15–23. doi:10.1002/nbm.3443.

High Temporospatial Resolution Dynamic Contrast Enhanced (DCE) Wrist MRI with Variable-Density Pseudo-Random CIRcular Cartesian UnderSampling (CIRCUS) Acquisition: Evaluation of Perfusion in Rheumatoid Arthritis Patients

Jing Liu, PhD[1], **Valentina Pedoia, PhD**[1], **Ursula Heilmeier, MD**[1], **Eric Ku, BS**[1], **Favian Su, BS**[1], **Sameer Khanna**[2], **John Imboden, MD**[3], **Jonathan Graf, MD**[3], **Thomas Link, MD**[1], and **Xiaojuan Li, PhD**[1]

[1]Department of Radiology and Biomedical Imaging, University of California San Francisco, San Francisco, California, United States

[2]University of California Berkeley, Berkeley, California, United States

[3]Department of Medicine, University of California San Francisco, San Francisco, California, United States

Abstract

This study is to evaluate highly accelerated 3D dynamic contrast-enhanced (DCE) wrist MRI for assessment of perfusion in rheumatoid arthritis (RA) patients. A pseudo-random variable-density undersampling strategy, CIRcular Cartesian UnderSampling (CIRCUS), was combined with k-t SPARSE-SENSE reconstruction to achieve a highly accelerated 3D DCE wrist MRI. Two healthy volunteers and ten RA patients were studied. Two patients were on methotrexate (MTX) only (Group I) and the other eight were treated with a combination therapy of MTX and Anti-Tumour Necrosis Factor (TNF) therapy (Group II). Patients were scanned at baseline and 3-month follow-up. DCE MR images were used to evaluate perfusion in synovitis and bone marrow edema pattern in the RA wrist joints. A series of perfusion parameters were derived and compared with clinical disease activity scores of 28 joints (DAS28). 3D DCE wrist MR images were obtained with a spatial resolution of $0.3\times0.3\times1.5mm^3$ and temporal resolution of 5 s (with an acceleration factor of 20). The derived perfusion parameters, most notably, transition time (dT) of synovitis, showed significant negative correlations with DAS28-ESR ($r=-0.80$, $p<0.05$) and DAS28-CRP ($r=-0.87$, $p<0.05$) at baseline and also correlated significantly with treatment responses evaluated by clinical score changes between baseline and 3-month follow-up (with DAS28-ESR: $r=-0.79$, $p<0.05$, and DAS28-CRP: $r=-0.82$, $p<0.05$). Highly accelerated 3D DCE wrist MRI with improved temporospatial resolution has been achieved in RA patients and provides accurate assessment of neovascularization and perfusion in RA joints, showing promise as a potential tool for evaluating treatment responses.

Corresponding Author Contact information Jing Liu, 185 Berry St, Suite 350, Radiology and Biomedical Imaging, University of California San Francisco, San Francisco, CA 94107, Tel: 415-514-8268 Fax: 415-353-9421, jing.liu@ucsf.edu.

Keywords

rheumatoid arthritis; perfusion; neovascularization; synovitis; dynamic contrast-enhanced; acceleration; undersampling; compressed sensing

INTRODUCTION

Rheumatoid arthritis (RA) is a chronic systemic inflammatory arthritis that affects 0.5-1.0% of adults, with 5~50 per 100,000 people newly developing the condition each year (1). RA most commonly occurs in the small joints of the hands, feet and cervical spine, but it can also involve larger joints such as the shoulder and knee. RA affects the synovium around the joints as well as the underlying bone and cartilage. It causes bony erosions, is associated with substantial pain and eventually leads to loss of joint function and long-term disability. Current clinical diagnosis of RA relies on patient symptoms and physical exams, as well as laboratory blood testing, synovial fluid and medical imaging including X-ray, Ultrasound and MRI. However, early diagnosis and prediction of RA progression is still challenging. Synovial angiogenesis has been proposed as one of the earliest markers of RA and magnetic resonance angiography (MRA) has been used as a noninvasive biomarker to identify abnormal vasculature in patients with early inflammatory arthritis (2, 3).

With the development of new treatments in the past decade to control joint inflammation and damage, the prognosis of RA has substantially improved (4-7). While non-pharmacological treatments that include physical therapy, splints and braces, occupational therapy and dietary changes are unable to stop the progression of joint destruction, biological medications that target inflammatory cytokines such as tumor necrosis factor alpha (TNF-alpha) can slow the progression of RA. However, their response varies among individual patients. It is then important to reliably identify patients at high risk for disease progression and accurately monitor their response to the treatments.

In previous studies, 3D dynamic contrast-enhanced (DCE) wrist magnetic resonance imaging (MRI) has been applied to evaluate perfusion changes in RA joints (2, 8, 9). The MRI perfusion curve reflects a composite of tissue perfusion, vessel permeability, and extravascular-extracellular space, which vary corresponding to tissue disease progression. An accurate assessment of neovascularization and perfusion in RA joints could enable earlier detection of RA and allow accurate monitoring of patient disease progression and treatment responses. However, current DCE wrist MRI techniques are limited to relatively low resolution (both spatial and temporal) which hinder their translation into clinical practice. In this study, we aim to develop and evaluate an improved DCE wrist MRI technique for accurate assessment of perfusion in RA joints.

Acceleration methods such as parallel imaging (PI) and compressed sensing (CS) techniques (10-16) have been proposed to reduce scan time and increase image quality with higher temporal and/or spatial resolution. Combined PI and CS techniques have been applied to DCE imaging in other organs such as brain (17), but haven’t been demonstrated for wrist DCE imaging yet. Theoretically, CS requires random undersampling for forming incoherent artifacts (13, 16), but in practice, pseudo-random undersampling is implemented. We have

proposed a novel pseudo-random variable-density undersampling strategy, CIRcular Cartesian UnderSampling (CIRCUS) (18-20), which integrates the desirable features of randomization, variable-density and interleaved trajectories on a 3D Cartesian grid. The time-resolved interleaving feature in CIRCUS allows for retrospective selection of temporal resolution. In this study, we combined our CIRCUS acquisition strategy with a k-t SPARSE-SENSE reconstruction method (21, 22) to obtain a highly accelerated 3D DCE wrist MRI in order to improve both spatial and temporal resolution for a more accurate assessment of perfusion in RA joints.

METHODS

Subjects

The study cohort is a sub-cohort of an ongoing prospective study. The study was approved by the Committee for Human Research at our institution. Written informed consent was obtained from all of the subjects after the nature of the study was fully explained.

Two healthy subjects (29.0 ± 5.7 years old, 1 female) and ten RA patients were imaged (51.3 ± 14.3 years old, 7 female, RA duration 46.4 ± 39.6 months). Two of the patients were on MTX only (Group I) and the other eight were on a combination therapy of MTX and anti-TNF (Group II). All patients were examined by rheumatologists (JI, 38 years in practice; JG, 18 years in practice) for tender joint count (TEN28), swollen joint count (SW28) and disease activity score of 28 joints (DAS28). On the same day of rheumatologist visit, serum samples were taken from the patients for erythrocyte sedimentation rate (ESR) and C-reactive protein (CRP) measurements.

Inclusion criteria required all patients to be ≥18 years at enrollment, able to give consent and follow the study protocol, and to fulfill the 2010 American College of Rheumatology (ACR) RA classification criteria. Prednisone was permitted at ≤10 mg daily. Specific inclusion criteria for Group I: DAS28 ≤3.2 during the last 2-months before the baseline visit, MTX treatment at a stable dose for > 8 weeks before baseline, no biologic treatment during the past 6-months before baseline and no anticipated biologic treatment. Specific inclusion criteria for Group II: DAS28 > 3.2, no biologic treatment during the past 6-months prior to the baseline visit and consent to initiate and maintain anti-TNF therapy with Certolizumab pegol (CIMZIA, UBC Inc. Smyrna, GA). Exclusion criteria for all study subjects included any inability to consent or perform a contrast enhanced MRI scan and any history of injury or surgery in the wrist or hand to be scanned.

MRI scans were performed on the same day as patient rheumatologist visits. Ten patients completed baseline scans and nine patients (2 in Group I and 7 in Group II) completed 3-month follow-up scans due to one patient becoming pregnant. For Group II patients, MRI scans were obtained directly before anti-TNF therapy initiation (baseline) and at 3-month follow-up after initiation.

MRI Data Acquisition

Data were acquired on a 3.0T MR scanner (GE Medical Systems, Milwaukee, WI) with an 8-channel phased array wrist coil. The total scan time was about 45 minutes, resulting in less than an hour for the entire MRI exam including setting up time.

CIRCUS was applied on the k_y-k_z plane of 3D Cartesian acquisitions (where k_x is the frequency encoding axis) and provides randomization, variable-density and flexible interleaving of the sampling points; features that are favorable for dynamic imaging combined with advanced image reconstruction methods such as in k-t, parallel imaging and compressed sensing (18). The golden-ratio profile used in CIRCUS allows for retrospective reconstruction with an arbitrary temporal resolution (18, 23). In this study, CIRCUS was implemented in a 3D gradient-echo sequence.

To validate the image quality with CIRCUS acquisition, we applied fully acquired k-space data on the conventional 3D gradient-echo sequence (SPGR) before contrast injection. The scan parameters for both sequences were: coronal view, FOV = 12×9 cm^2, TR/TE = 11.1/2.5 ms, FA = 20°, BW = ± 62.5 kHz, image matrix = 384×288, 28~32 slices, spatial resolution = 0.3×0.3×1.5 mm^3. The scan time of the conventional SPGR acquisition before contrast injection was ~100s, immediately followed by the dynamic contrast enhanced SPGR with CIRCUS acquisition (~400 s) with a 40 s injection delay (Gd-DTPA, 0.2mmol/kg).

T_2-weighted IDEAL Fast-Spin Echo (FSE) images were acquired in coronal and axial planes before applying the conventional 3D SPGR imaging. Scan parameters include: FOV = 12×9 cm^2, TR/TE = 3806/53 ms, FA = 90°, BW = ±195 kHz, image matrix = 512×512, 20 slices, and spatial resolution = 0.23×0.23×2.0 mm^3. T_1-weighted IDEAL FSE images in coronal view were acquired before and after the conventional 3D SPGR and DCE imaging. Scan parameters include: FOV = 12×9 cm^2, TR/TE = 500/12 ms, FA = 111°, BW = ±195 kHz, image matrix = 512×512, 20 slices, and spatial resolution = 0.23×0.23×2.0 mm^3.

Data Processing

MRI data were saved and images were reconstructed off-line using MATLAB (The MathWorks, Natick, MA) on a Macintosh with an Intel Core i7 Processor (3.1 GHz). Fully acquired k-space 3D SPGR data were reconstructed by applying inverse Fourier Transformation with the images as reference. DCE data with CIRCUS acquisition were reconstructed with retrospectively chosen temporal resolutions: 10 s (corresponding to an acceleration factor of R=10) and 5 s (R=20). Data were reconstructed with k-t SPARSE-SENSE reconstruction method (21, 22) in which the undersampled data sets were reconstructed with multi-coil CS that exploits joint sparsity along the temporal dimension by using a total variation constraint in this study.

DCE baseline images (images acquired during the 40 s injection delay) obtained with CIRCUS acquisition were compared with the reference images (acquired with fully sampled data before administration of contrast injection) by calculating the Normalized Root-Mean-

Square Error (NRMSE) defined as $\frac{\sqrt{\left(\sum_{i=0}^{N-1}\left(x_1(i)-x_2(i)\right)^2\right)/N}}{max(x_1)-min(x_1)}$ (16) , where x_1 is the reference measurement and x_2 is the measurement to evaluate.

DCE as well as T_2-weighted IDEAL Fast Spin Echo (Water) images were non-rigidly aligned to the first time point (baseline image) of DCE. Non-rigid registration was developed using elastix ITK (Insight Segmentation and Registration Toolkit) library (24-26). An intensity based five-level multi-resolution pyramidal approach was applied to accomplish the registration task. B-spline transformation was used for the morphing and final interpolation and Advance Mattes Mutual Information was used as a figure of merit of the transformation and iteratively optimized. The difference between the fixed image (first time point) and all the other was qualitatively checked to evaluate the performance of the registration procedure.

Region of interests (ROIs) including synovitis (SYN) and bone marrow edema pattern (BMEP) were identified in IDEAL images semi-automatically using in-house developed software (8, 27). Their mean signal intensities throughout time (signal-time curves) were measured to calculate six perfusion parameters:

1. maximum intensity: MaxI (%), relative to baseline image;
2. transition time: dT (s), time between 20% and 80% MaxI;
3. slope: Slope (%/min) = MaxI·(80%-20%)/(dT/60);
4. time to peak: TTP (s);
5. area under the curve: AUC (%·hour); and
6. area under the curve before TTP: AUCP (%·hour).

Fig.1 demonstrates how the perfusion parameters (except slope) are defined.

OMERACT RA MRI Scoring (RAMRIS) was performed by a musculoskeletal radiologist (TL, 23 years of experience) for all MR studies at baseline and follow-up (28, 29). Synovitis volume scores (SYN grading) were obtained based on pre- and post-contrast T_1-weighted IDEAL images.

Statistical Analysis

A two-tailed paired-sample t-test was used to compare the clinical disease activity scores and perfusion parameters between baseline and 3-month follow-up. P-values of less than 0.05 were considered statistically significant. Pearson correlation coefficients between perfusion parameters and clinical disease activity scores were calculated at baseline. Pearson correlation coefficients between the changes of perfusion parameters and those of clinical disease activity scores from baseline to 3-month follow-up were evaluated. P-values were calculated based on 95% confident intervals ($p<0.05$, correlation is significant). SYN grading was analyzed and compared with DAS28 and the perfusion parameters.

RESULTS

Fig.2 compares DCE baseline images and the reference images acquired with fully sampled data before administration of contrast injection. NRMSEs from baseline scans were 4.0 ± 2.5% and 4.1±2.3% for data sets with 10 s and 5 s temporal resolution respectively.

In Fig.3, DCE maximum intensity projection (MIP) images show the neovascularization at early venous phase (middle column), as well as synovitis and contrast agent leakage at late-venous phase (right column) in two RA patients (second and third rows) compared with the clear joints of a healthy volunteer (first row). Patients' score were DAS-ESR=2.9, DAS-CRP=1.2 (second row), and DAS-ESR=6.0, DAS-CRP=5.5 (third row).

Table 1 summarizes the patients' clinical disease activity scores at baseline and 3-month follow-up rheumatologist visits. Significant changes (t-test, $p<0.05$) between baseline and 3-month follow-up disease activity scores including TEN28, SW28, and DAS28-ESR are highlighted in bold and marked with *.

At baseline, nine out of ten patients showed SYN and BME. At 3-month follow-up, eight out of nine patients had SYN and BME. Table 2a&b list the perfusion parameters that were derived from the time-signal curves of selected ROIs of SYN and BME respectively, evaluated with both 10 s and 5 s temporal resolution. No significant differences in perfusion parameters in SYN and BMEP between baseline and 3-month follow-up were observed in this cohort.

The correlations between the clinical disease activity scores and the perfusion parameters of SYN at baseline are reported in Table 3. The transition time (dT), maximum intensity (MaxI) and area under the curve (AUC) of synovitis were found to be highly correlated with clinical disease activity scores except ESR and CRP that were obtained from blood tests. The transition time dT outperformed the other perfusion parameters by providing higher correlations. Although 10 s and 5 s data sets produced similar results, the higher temporal resolution (5 s) can improve the correlations between the transition time dT of SYN and the clinical disease activity scores (with TEN28, from r=-0.85 to -0.95; with DAS28-CRP, from r=0.70 to -0.87); even making non-significant correlations significant (with SW28, from r=0.59 to 0.77; with DAS28-ESR, from r=-0.53 to -0.80).

Changes between baseline and 3-month follow-up in SYN perfusion parameters were evaluated and compared with changes in clinical disease activity scores (Table 4). Significant correlations are only found between changes in some of the SYN perfusion parameters with changes in TEN28, SW28, DAS28-ESR, and DAS28-CRP (Table 4, numbers highlighted in bold and marked with *). We found significant negative correlations between changes in transition time (dT) of SYN with 5 s temporal resolution and changes in global clinical disease activity scores DAS28-ESR (r=-0.79. p-value =0.02) and DAS28-CRP (r=-0.82, p-value =0.01). Fig. 4 shows the corresponding scatter plots of 8 patient data points, between dT measurements and DAS28-ESR scores (Fig. 4a), as well as between dT and DAS28-CRP (Fig. 4b). Group I (without anti-TNF treatment) patients showed an increase in clinical disease activity scores (Fig. 4, marked with asterisks) while Group II (with anti-TNF treatment) patients showed a decrease (Fig. 4, marked with circles).

The clinical SYN grading only showed correlations with SW28 and DAS28-ESR at baseline (Table 3, last column on the right). However, this conventional clinical SYN grading based on MRI failed to monitor patient disease activity changes (Table 4, last column on the right).

We also evaluated the correlations between the BME perfusion parameters and clinical disease activity scores. At baseline, the area under the curve before time to peak (AUCP) of BMEP showed high correlations ($r>0.70$, negative) with some of the clinical disease activity scores (TEN28, DAS28-ESR, and DAS28-CRP). However, no significant correlations were found between baseline and 3-month follow-up changes.

Fig. 5 shows DCE MIP images from a patient from Group II with improved RA symptoms following therapy (TEN28 changed from 17.0 to 0.0, SW28 from 14.0 to 3.0, ESR from 38.0 to 27.0, CRP from 20.1 to 5.6, DAS28-ESR from 6.6 to 2.8, DAS28-CRP from 6.1 to 2.1, SYN grading from 6.0 to 3.0, and dT of SYN from 41.6 s to 127.7 s). The enhancing regions in the wrist were significantly reduced at 3-month follow-up (Fig. 5b) compared to those at baseline (Fig. 5a). The contrast enhancements of SYN and BME (measured in the ROI shown in Fig. 6b&c) were slower and lower at 3-month follow-up compared to those at baseline (Fig. 6e). The higher temporal resolution (5s) provides a better capture of the signal change during contrast injection, especially in arterial blood (Fig. 6e).

DISCUSSION AND CONCLUSION

In this study, high temporospatial DCE wrist MRI with a temporal resolution of 5 s and spatial resolution of $0.3\times0.3\times1.5$ mm^3 was successfully applied to evaluate neovascularization and perfusion in RA patients. Previous studies reported using DCE wrist MRI for perfusion changes in RA with temporal and spatial resolutions of 12 s and $0.4\times0.4\times3$ mm^3 (8), and 10.3 s and 1.25mm×1.25 mm×0.63 mm^3 (9). Our method uses a temporal and spatial resolution of 5 s and $0.3\times0.3\times1.5$ mm^3 improves temporospatial resolution by an overall factor of R=8.5 and R=15 when compared to these two previous studies respectively. The low error between the images obtained with undersampled data and the fully-sample reference images demonstrates that comparable image quality can be obtained with CIRCUS acquisition to the reference even with a large acceleration factor of R=20. This is our first attempt to apply the proposed acceleration method for wrist MRI. Other applications include 3D cardiac cine MRI and intracranial 4D flow MRI (19, 20).

In designing our accelerated technique, we chose to improve the spatial and temporal resolutions rather than reduce the overall scan time because we wanted to ensure adequate coverage of the contrast enhancement in RA joints as shown in literature (6~7 minutes). Higher spatial resolution will improve the characterization of small lesion perfusion properties and in heterogeneous tissues and lesions. Higher temporal resolution reconstruction provides more accurate tracking of the signal change during contrast injection. This highly accelerated acquisition provides a comprehensive overview of the arterial and venous phases and detailed estimations of perfusion changes in time over a full 3D volume. We demonstrate that perfusion measurements (especially the transition time dT) in synovitis of RA joints can accurately monitor patient's response to the treatments. Although we limited the analysis to empirical calculation of perfusion parameters from the

time-intensity curve, implementing pharmacokinetic models for perfusion in RA will be interesting to investigate in the future (30, 31) and high temporal resolution will help to increase the robustness and reliability of such modeling (32, 33).

In our current study, we measured the perfusion within selected ROIs, which were segmented based on T2-weighted IDEAL images. With higher spatial resolution, we can achieve better image registration between the IDEAL and DCE images. And we can have more accurate ROI segmentation with less partial volume effect. Non-rigid registration in this study was developed using elastix library, which is characterized by a highly modular structure and allows for building highly efficacious algorithms. All the basic steps of a classical registration pipeline can be customized by choosing the best combination of image similarity metric, optimization algorithm and interpolation strategy. Multiresolution hierarchical approaches were available to strike a good balance between algorithm performance and execution time demands.

Patients in Group II with anti-TNF therapy showed a decrease in clinical disease activity scores, indicating positive response to treatment. However, there is a large variation of treatment responses among patients. Using the EULAR treatment response criteria (34), two patients showed good responses; three patients showed moderate response; and one patient showed no response. Such variations suggest the pressing clinical need for reliable evaluation and quantification of treatment response.

Although not significant, the maximum enhancement MaxI of both synovitis and bone marrow edema pattern reduced after anti-TNF treatment which is consistent with previous reports in the literature (35). The synovitis perfusion evaluation (transition time dT, Tables 3&4) was significantly correlated with DAS28 changes while the synovitis grading was not. This suggests that quantitative perfusion evaluation outperforms clinical synovitis grading in detecting changes (sometimes can be subtle) after treatment and that quantitative DCE wrist MRI can be used as a more reliable and accurate tool for evaluating RA treatment response, which is currently applied in clinical studies to assess its potential role in optimizing treatment decisions.

At baseline, significant correlation was found between DCE parameters of SYN/BME and RAMRIS grading of SYN/BME. Such correlation was previously reported by Boesen et al and the investigators suggested that computer-aided perfusion analysis may be useful for quick semi-automated assessment of joint inflammation as it took significantly shorter time compared to RAMRIS grading (36). In the study reported by Cimmino et al (37), in 10 patients treated with rituximab (another type of anti-TNF treatment), SYN perfusion parameters but not SYN RAMRIS grading significantly were correlated with DAS at baseline, 1- and 6-months after treatment. In our study, we further observed that only SYN DCE parameter changes, but not SYN RAMRIS grading changes, were correlated with DAS changes after treatment. These results suggest that quantitative perfusion evaluation outperforms clinical synovitis grading.

The correlation between synovitis and clinical evaluation we observed is consistent with the literature where synovitis measured by MRI or ultrasound, or metabolic activity of synovitis

measured by PET imaging were correlated with clinical evaluations in RA (38-40). At baseline, the perfusion parameters of bone marrow edema pattern were correlated with some of the clinical disease activity scores. The changes of bone marrow edema pattern perfusion parameters, however, were not correlated with the changes in clinical disease activity scores. This is in contrast to the synovitis perfusion parameters and suggests that synovitis is more directly linked with clinical evaluations such as DAS28 (which include the touch and feel of the swollen of the joints); while bone marrow edema pattern is more indicative of inflammatory-related changes within bone and bone marrow. This is supported by previous studies in which bone marrow edema pattern has been shown to be a strong predictor of radiographic erosion development in RA joints (41-43). We will be following the same cohort of patients up to 1-year after anti-TNF initiation and the DCE data will be used to evaluate the longitudinal correlation between bone marrow edema pattern perfusion parameters and erosion development.

We are aware that this study has several limitations. In this study, a limited number of patients have been involved for demonstrating the improvements of perfusion evaluation in RA with our new DCE wrist MRI technique. In the future, a larger group of patients is desired for a more comprehensive evaluation of the technique. We are also aware that RA duration of the patients involved in this study was heterogeneous (46.4 ± 39.6 months). We have derived perfusion parameters directly from the DCE time-signal curves. Such parameters are defined as “semi-quantitative” perfusion parameters, because they provide “relative” access to the physiologic parameters. While “quantitative” perfusion parameters may be derived by integrating the arterial input function, which takes into account physiologic variations such as the blood flow, the vascular structure, and so on. We are currently working on delivering quantitative perfusion parameters. With high temporospatial DCE imaging, it is expected to have a more accurate arterial input function (demonstrated in Fig. 6), which is crucial for achieving accurate perfusion measurements. Currently DCE data is reconstructed offline with MATLAB-based programming. Images with 40 time points (10s temporal resolution) took about 8 hours of reconstruction time, and those with 80 time points (5s) took about 30 hours computation time on a Macintosh with an Intel Core i7 Processor (3.1 GHz). The reconstruction definitely needs future optimization to be clinically practical.

In conclusion, highly accelerated 3D DCE wrist MRI has been achieved in RA patients with improved temporospatial resolution, which provides accurate quantitative assessment of neovascularization and perfusion in RA joints. Such technique improved monitoring of treatment response and disease progression, thus has the great potential to optimize treatment strategy for patients with RA.

Acknowledgments

This work was supported in part by grant from UCB Inc (XL) and NIH K25EB014914 (JL).

References

1. Scott DL, Wolfe F, Huizinga TW. Rheumatoid arthritis. Lancet. 2010; 376(9746):1094–108.10.1016/S0140-6736(10)60826-4 [PubMed: 20870100]

2. Vasanth LC, Foo LF, Potter HG, Adler RS, Finzel KC, Pavlov H, Mandl LA. Using magnetic resonance angiography to measure abnormal synovial blood vessels in early inflammatory arthritis: a new imaging biomarker? The Journal of rheumatology. 2010; 37(6):1129–35.10.3899/jrheum.090063 [PubMed: 20360190]

3. Gaffney K, Cookson J, Blades S, Coumbe A, Blake D. Quantitative assessment of the rheumatoid synovial microvascular bed by gadolinium-DTPA enhanced magnetic resonance imaging. Annals of the rheumatic diseases. 1998; 57(3):152–7. [PubMed: 9640130]

4. Kingsley G, Scott IC, Scott DL. Quality of life and the outcome of established rheumatoid arthritis. Best practice & research Clinical rheumatology. 2011; 25(4):585–606.10.1016/j.berh.2011.10.003 [PubMed: 22137926]

5. Lipsky PE, van der Heijde DM, St Clair EW, Furst DE, Breedveld FC, Kalden JR, Smolen JS, Weisman M, Emery P, Feldmann M, Harriman GR, Maini RN. Anti-Tumor Necrosis Factor Trial in Rheumatoid Arthritis with Concomitant Therapy Study G. Infliximab and methotrexate in the treatment of rheumatoid arthritis. Anti-Tumor Necrosis Factor Trial in Rheumatoid Arthritis with Concomitant Therapy Study Group. The New England journal of medicine. 2000; 343(22):1594–602.10.1056/NEJM200011303432202 [PubMed: 11096166]

6. Breedveld FC, Weisman MH, Kavanaugh AF, Cohen SB, Pavelka K, van Vollenhoven R, Sharp J, Perez JL, Spencer-Green GT. The PREMIER study: A multicenter, randomized, double-blind clinical trial of combination therapy with adalimumab plus methotrexate versus methotrexate alone or adalimumab alone in patients with early, aggressive rheumatoid arthritis who had not had previous methotrexate treatment. Arthritis and rheumatism. 2006; 54(1):26–37.10.1002/art.21519 [PubMed: 16385520]

7. Genovese MC, Bathon JM, Martin RW, Fleischmann RM, Tesser JR, Schiff MH, Keystone EC, Wasko MC, Moreland LW, Weaver AL, Markenson J, Cannon GW, Spencer-Green G, Finck BK. Etanercept versus methotrexate in patients with early rheumatoid arthritis: two-year radiographic and clinical outcomes. Arthritis and rheumatism. 2002; 46(6):1443–50.10.1002/art.10308 [PubMed: 12115173]

8. Li X, Yu A, Virayavanich W, Noworolski SM, Link TM, Imboden J. Quantitative characterization of bone marrow edema pattern in rheumatoid arthritis using 3 Tesla MRI. Journal of magnetic resonance imaging : JMRI. 2012; 35(1):211–7.10.1002/jmri.22803 [PubMed: 21987483]

9. Rastogi A, Kubassova O, Krasnosselskaia LV, Lim AK, Satchithananda K, Boesen M, Binks M, Hajnal JV, Taylor PC. Evaluating automated dynamic contrast enhanced wrist 3T MRI in healthy volunteers: one-year longitudinal observational study. European journal of radiology. 2013; 82(8):1286–91.10.1016/j.ejrad.2013.02.041 [PubMed: 23562303]

10. Donoho DL. Compressed sensing. IEEE Transactions on Information Theory. 2006; 52:1289–306.

11. Candes EJ, Romberg J, Tao T. Robust uncertainty principles: Exact signal reconstruction from highly incomplete frequency information. IEEE Transactions on Information Theory. 2006; 52:489–509.

12. Candes EJ, Tao T. Near-optimal signal recovery from random projections: Universal encoding strategies? IEEE Transactions on Information Theory. 2006; 52:5406–25.

13. Lustig M, Donoho D, Pauly JM. Sparse MRI: The application of compressed sensing for rapid MR imaging. Magnetic resonance in medicine : official journal of the Society of Magnetic Resonance in Medicine / Society of Magnetic Resonance in Medicine. 2007; 58(6):1182–95. Epub 2007/10/31. 10.1002/mrm.21391

14. Pruessmann KP, Weiger M, Scheidegger MB, Boesiger P. SENSE: sensitivity encoding for fast MRI. Magn Reson Med. 1999; 42(5):952–62. [PubMed: 10542355]

15. Griswold MA, Jakob PM, Heidemann RM, Nittka M, Jellus V, Wang J, Kiefer B, Haase A. Generalized autocalibrating partially parallel acquisitions (GRAPPA). Magn Reson Med. 2002; 47(6):1202–10. [PubMed: 12111967]

16. Lustig M, Pauly JM. SPIRiT: Iterative self-consistent parallel imaging reconstruction from arbitrary k-space. Magnetic resonance in medicine : official journal of the Society of Magnetic Resonance in Medicine / Society of Magnetic Resonance in Medicine. 2010; 64(2):457–71. Epub 2010/07/29. 10.1002/mrm.22428

17. Lebel RM, Jones J, Ferre JC, Law M, Nayak KS. Highly accelerated dynamic contrast enhanced imaging. Magnetic resonance in medicine : official journal of the Society of Magnetic Resonance

in Medicine / Society of Magnetic Resonance in Medicine. 2014; 71(2):635–44.10.1002/mrm.24710

18. Liu J, Saloner D. Accelerated MRI with CIRcular Cartesian UnderSampling (CIRCUS): a variable density Cartesian sampling strategy for compressed sensing and parallel imaging. Quantitative imaging in medicine and surgery. 2014; 4(1):57–67.10.3978/j.issn.2223-4292.2014.02.01 [PubMed: 24649436]
19. Liu, J.; Feng, L.; Saloner, D. Highly Accelerated Free-breathing 4D Cardiac Imaging with CIRCUS Acquisition. Proceedings of the 22nd Annual Meeting of ISMRM; Milan, Italy. 2014. p. 429
20. Liu, J.; Faraji, F.; Kefayati, S.; Haraldsson, H.; Saloner, D. Highly Accelerated Intracranial 4D Flow MRI with CIRcular Cartesian UnderSampling (CIRCUS). Proceedings of the 23rd Annual Meeting of ISMRM; Toronto, Canada. 2015. p. 458
21. Otazo R, Kim D, Axel L, Sodickson DK. Combination of compressed sensing and parallel imaging for highly accelerated first-pass cardiac perfusion MRI. Magn Reson Med. 2010; 64(1):767–76. Epub 2010/06/11. 10.1002/mrm.22463 [PubMed: 20535813]
22. Feng L, Srichai MB, Lim RP, Harrison A, King W, Adluru G, Dibella EV, Sodickson DK, Otazo R, Kim D. Highly accelerated real-time cardiac cine MRI using k-t SPARSE-SENSE. Magn Reson Med. 2013; 70(1):64–74.10.1002/mrm.24440 [PubMed: 22887290]
23. Winkelmann S, Schaeffter T, Koehler T, Eggers H, Doessel O. An optimal radial profile order based on the Golden Ratio for time-resolved MRI. IEEE Trans Med Imaging. 2007; 26(1):68–76. [PubMed: 17243585]
24. Klein S, Staring M, Murphy K, Viergever MA, Pluim JP. elastix: a toolbox for intensity-based medical image registration. IEEE transactions on medical imaging. 2010; 29(1):196–205.10.1109/TMI.2009.2035616 [PubMed: 19923044]
25. Shamonin DP, Bron EE, Lelieveldt BP, Smits M, Klein S, Staring M. Alzheimer's Disease Neuroimaging I. Fast parallel image registration on CPU and GPU for diagnostic classification of Alzheimer's disease. Frontiers in neuroinformatics. 2013; 7:50.10.3389/fninf.2013.00050 [PubMed: 24474917]
26. Gubern-Merida A, Marti R, Melendez J, Hauth JL, Mann RM, Karssemeijer N, Platel B. Automated localization of breast cancer in DCE-MRI. Medical image analysis. 2015; 20(1):265–74.10.1016/j.media.2014.12.001 [PubMed: 25532510]
27. Yang H, Rivoire J, Hoppe M, Srikhum W, Imboden J, Link TM, Li X. Computer-aided and manual quantifications of MRI synovitis, bone marrow edema-like lesions, erosion and cartilage loss in rheumatoid arthritis of the wrist. Skeletal radiology. 201410.1007/s00256-014-2059-3
28. Lassere M, McQueen F, Ostergaard M, Conaghan P, Shnier R, Peterfy C, Klarlund M, Bird P, O'Connor P, Stewart N, Emery P, Genant H, Edmonds J. OMERACT Rheumatoid Arthritis Magnetic Resonance Imaging Studies. Exercise 3: an international multicenter reliability study using the RA-MRI Score. The Journal of rheumatology. 2003; 30(6):1366–75. [PubMed: 12784419]
29. Ostergaard M, Peterfy C, Conaghan P, McQueen F, Bird P, Ejbjerg B, Shnier R, O'Connor P, Klarlund M, Emery P, Genant H, Lassere M, Edmonds J. OMERACT Rheumatoid Arthritis Magnetic Resonance Imaging Studies. Core set of MRI acquisitions, joint pathology definitions, and the OMERACT RA-MRI scoring system. The Journal of rheumatology. 2003; 30(6):1385–6. [PubMed: 12784422]
30. Hodgson RJ, Connolly S, Barnes T, Eyes B, Campbell RS, Moots R. Pharmacokinetic modeling of dynamic contrast-enhanced MRI of the hand and wrist in rheumatoid arthritis and the response to anti-tumor necrosis factor-alpha therapy. Magnetic resonance in medicine : official journal of the Society of Magnetic Resonance in Medicine / Society of Magnetic Resonance in Medicine. 2007; 58(3):482–9.10.1002/mrm.21349
31. Hodgson RJ, Barnes T, Connolly S, Eyes B, Campbell RS, Moots R. Changes underlying the dynamic contrast-enhanced MRI response to treatment in rheumatoid arthritis. Skeletal radiology. 2008; 37(3):201–7.10.1007/s00256-007-0408-1 [PubMed: 18058095]
32. Michaely HJ, Sourbron SP, Buettner C, Lodemann KP, Reiser MF, Schoenberg SO. Temporal constraints in renal perfusion imaging with a 2-compartment model. Investigative radiology. 2008; 43(2):120–8.10.1097/RLI.0b013e3181583b0c [PubMed: 18197064]

33. Heisen M, Fan X, Buurman J, van Riel NA, Karczmar GS, ter Haar Romeny BM. The influence of temporal resolution in determining pharmacokinetic parameters from DCE-MRI data. Magnetic resonance in medicine : official journal of the Society of Magnetic Resonance in Medicine / Society of Magnetic Resonance in Medicine. 2010; 63(3):811–6.10.1002/mrm.22171
34. Fransen J, van Riel PL. The Disease Activity Score and the EULAR response criteria. Clinical and experimental rheumatology. 2005; 23(5 Suppl 39):S93–9. [PubMed: 16273792]
35. Haavardsholm EA, Ostergaard M, Hammer HB, Boyesen P, Boonen A, van der Heijde D, Kvien TK. Monitoring anti-TNFalpha treatment in rheumatoid arthritis: responsiveness of magnetic resonance imaging and ultrasonography of the dominant wrist joint compared with conventional measures of disease activity and structural damage. Annals of the rheumatic diseases. 2009; 68(10):1572–9.10.1136/ard.2008.091801 [PubMed: 19019893]
36. Boesen M, Kubassova O, Bouert R, Axelsen MB, Ostergaard M, Cimmino MA, Danneskiold-Samsoe B, Horslev-Petersen K, Bliddal H. Correlation between computer-aided dynamic gadolinium-enhanced MRI assessment of inflammation and semi-quantitative synovitis and bone marrow oedema scores of the wrist in patients with rheumatoid arthritis--a cohort study. Rheumatology. 2012; 51(1):134–43.10.1093/rheumatology/ker220 [PubMed: 22075065]
37. Cimmino MA, Parodi M, Zampogna G, Boesen M, Kubassova O, Barbieri F, Paparo F, Garlaschi G, Cutolo M. Dynamic contrast-enhanced, extremity-dedicated MRI identifies synovitis changes in the follow-up of rheumatoid arthritis patients treated with rituximab. Clinical and experimental rheumatology. 2014; 32(5):647–52. [PubMed: 25068921]
38. Goupille P, Roulot B, Akoka S, Avimadje AM, Garaud P, Naccache L, Le Pape A, Valat JP. Magnetic resonance imaging: a valuable method for the detection of synovial inflammation in rheumatoid arthritis. The Journal of rheumatology. 2001; 28(1):35–40. [PubMed: 11196540]
39. Zufferey P, Brulhart L, Tamborrini G, Finckh A, Scherer A, Moller B, Ziswiler HR. Ultrasound evaluation of synovitis in RA: correlation with clinical disease activity and sensitivity to change in an observational cohort study. Joint, bone, spine : revue du rhumatisme. 2014; 81(3):222–7.10.1016/j.jbspin.2013.08.006
40. Beckers C, Ribbens C, Andre B, Marcelis S, Kaye O, Mathy L, Kaiser MJ, Hustinx R, Foidart J, Malaise MG. Assessment of disease activity in rheumatoid arthritis with (18)F-FDG PET. Journal of nuclear medicine : official publication, Society of Nuclear Medicine. 2004; 45(6):956–64.
41. McQueen FM, Benton N, Perry D, Crabbe J, Robinson E, Yeoman S, McLean L, Stewart N. Bone edema scored on magnetic resonance imaging scans of the dominant carpus at presentation predicts radiographic joint damage of the hands and feet six years later in patients with rheumatoid arthritis. Arthritis and rheumatism. 2003; 48(7):1814–27.10.1002/art.11162 [PubMed: 12847674]
42. Haavardsholm EA, Boyesen P, Ostergaard M, Schildvold A, Kvien TK. Magnetic resonance imaging findings in 84 patients with early rheumatoid arthritis: bone marrow oedema predicts erosive progression. Annals of the rheumatic diseases. 2008; 67(6):794–800.10.1136/ard.2007.071977 [PubMed: 17981915]
43. Hetland ML, Stengaard-Pedersen K, Junker P, Ostergaard M, Ejbjerg BJ, Jacobsen S, Lottenburger T, Hansen I, Tarp U, Andersen LS, Svendsen A, Pedersen JK, Lauridsen UB, Ellingsen T, Lindegaard H, Podenphant J, Vestergaard A, Jurik AG, Horslev-Petersen K. group Cs. Radiographic progression and remission rates in early rheumatoid arthritis - MRI bone oedema and anti-CCP predicted radiographic progression in the 5-year extension of the double-blind randomised CIMESTRA trial. Annals of the rheumatic diseases. 2010; 69(10):1789–95.10.1136/ard.2009.125534 [PubMed: 20444751]

Abbreviations

MRI	magnetic resonance imaging
DCE	dynamic contrast-enhanced
3D	three-dimensional
CIRCUS	circular Cartesian undersampling

RA	rheumatoid arthritis
SENSE	sensitivity encoding
MTX	methotrexate
TNF	anti-tumour necrosis factor
DAS28	disease activity scores of 28 joints
ESR	erythrocyte sedimentation rate
CRP	C-reactive protein
TEN	tender joint count
SW	swollen joint count
MRA	magnetic resonance angiography
PI	parallel imaging
CS	compressed sensing
ACR	American College of Rheumatology
SPGR	gradient-echo sequence
Gd-DTPA	gadolinium-diethylenetriamine pentaacetic acid
IDEAL	iterative decomposition of water and fat with echo asymmetry and least-squares estimation
FSE	Fast-Spin Echo
FOV	field of view
TR	repetition time
TE	echo time
FA	flip angle
BW	bandwidth
NRMSE	normalized root-mean-square error
ITK	Insight Segmentation and Registration Toolkit
ROI	region of interests
SYN	synovitis
BME	bone marrow edema
BMEP	bone marrow edema pattern
MaxI	maximum intensity
dT	transition time
TTP	time to peak

AUC	area under the curve
AUCP	area under the curve before TTP
OMERACT	outcome measures for arthritis clinical trials
RAMRIS	rheumatoid arthritis MRI scoring system
EULAR	European league against rheumatism
MIP	maximum intensity projection

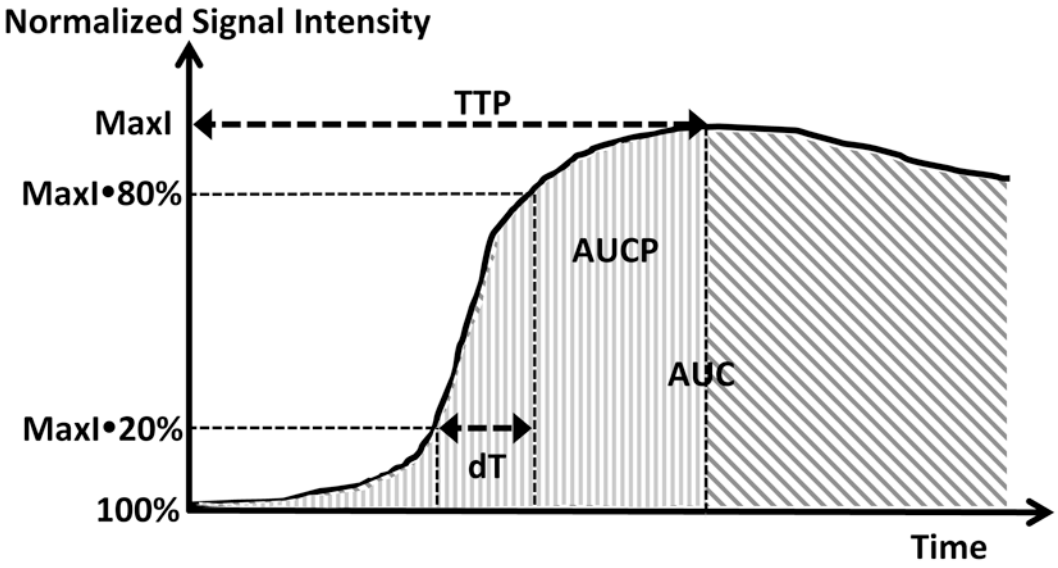

Figure 1.

Perfusion parameters derived from DCE signal-time curve. The entire curve is normalized relative to the baseline signal (100%). Six perfusion parameters are derived from the curve. MaxI: maximum intensity (%), dT: transition time (s), time between 20% and 80% MaxI); slope: MaxI(80%-20%)/(dT/60) (%/min) (not shown); TTP: time to peak (s); AUC: area under the curve (%hour); and AUCP: area under the curve before TTP (%hour).

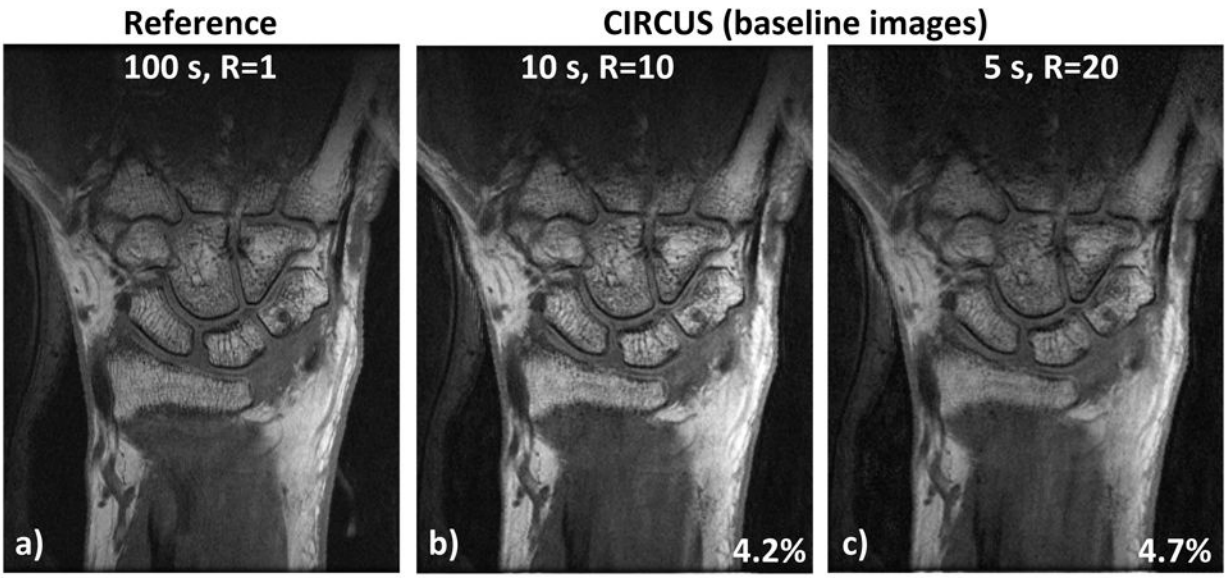

Figure 2.

Comparison of highly accelerated images with the reference. Even with acceleration factor of **b)** 10 or **c)** 20, CIRCUS provides comparable image quality to **a)** the reference. Normalized root-mean-square errors of the images obtained with CIRCUS are relatively low compared to the reference.

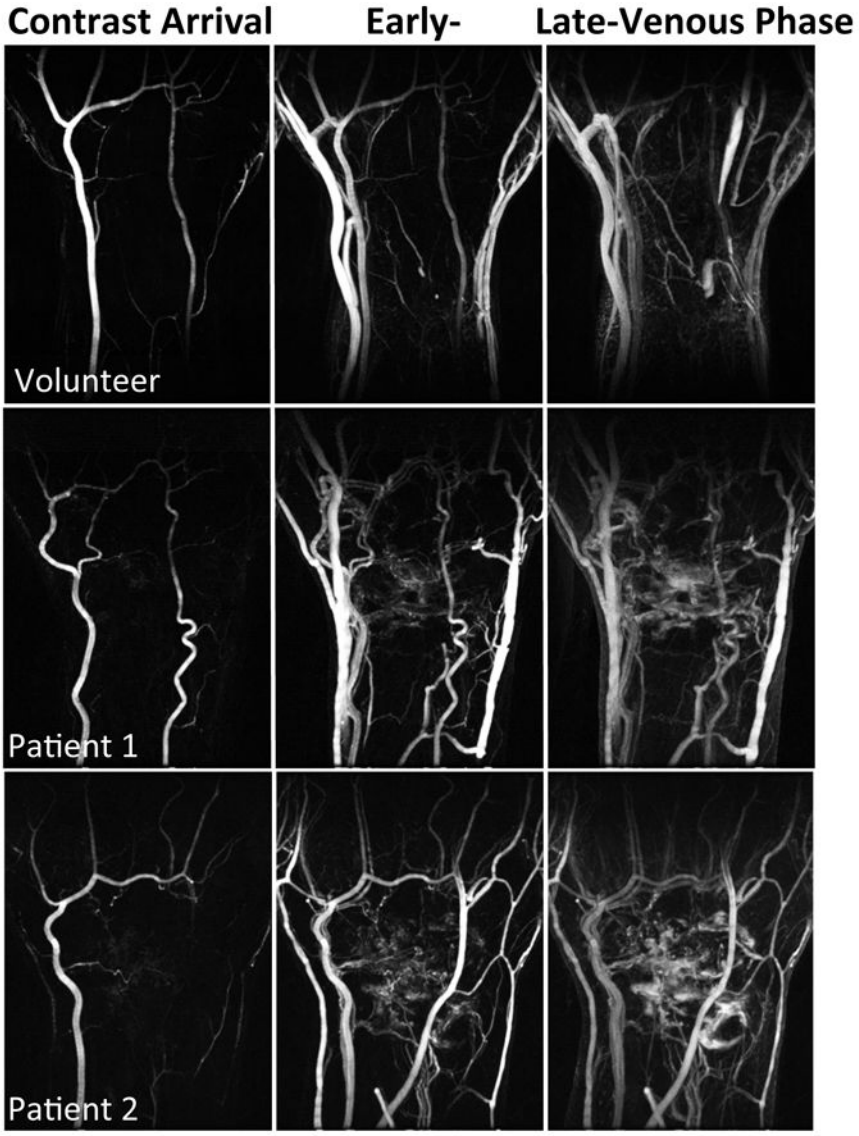

Figure 3.

MIP images at three representative time frames of a temporal resolution 5 s. Patient 1 has DAS28-ESR score of 2.9 and DAS28-CRP score of 1.2 (low disease activity), and RA duration of 57.8 months. Patient 2 has DAS28-ESR score of 6.0 and DAS28-CRP score of 5.5 (high disease activity), and RA duration of 117.3 months.

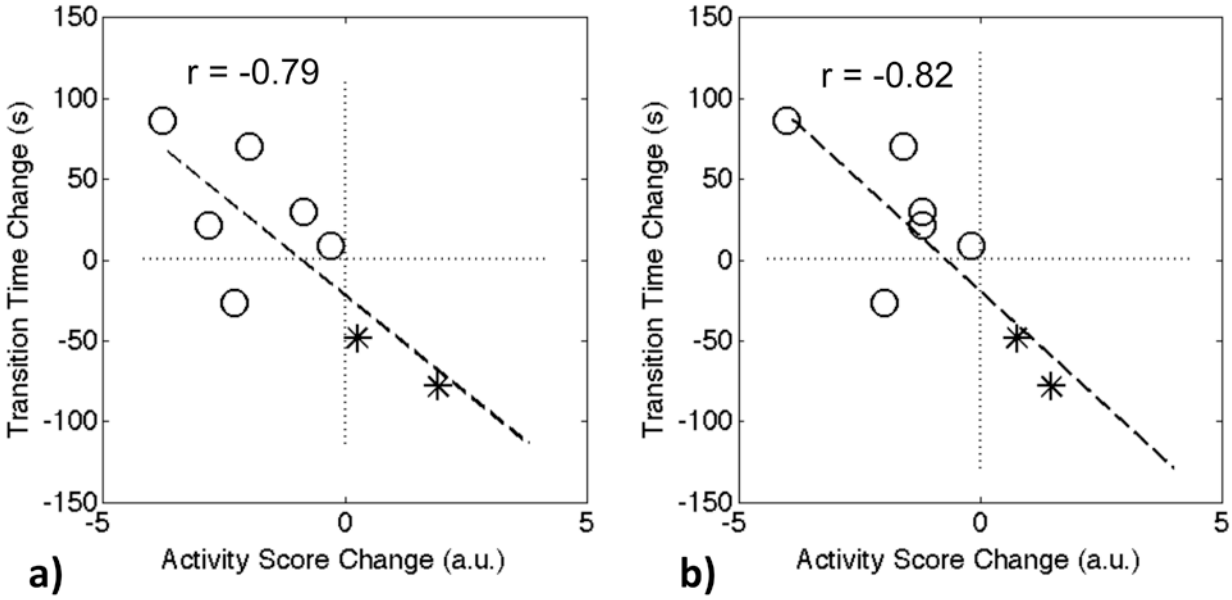

Figure 4.

The change of the transition time dT in synovitis (5 s resolution) between the baseline and 3-month follow-up scans is highly correlated with the change of the activity score, **a)** DAS28-ESR, and **b)** DAS28-CRP. The data points marked with circles are Group II patients, and the rest two points marked with asterisks denote Group I patients.

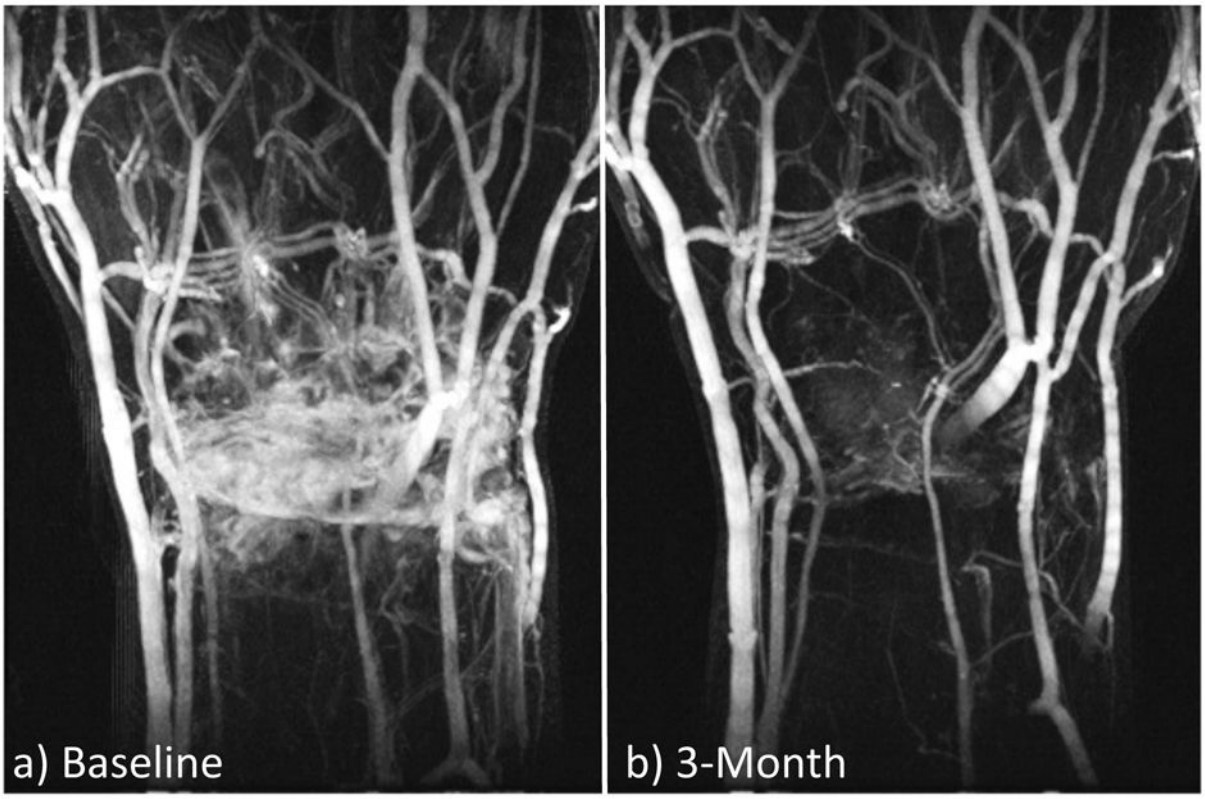

Figure 5.
DCE MIP images at **a)** baseline and **b)** 3-month follow-up with a temporal resolution of 5s. Data is from a Group II patient, who had good positive response to treatment.

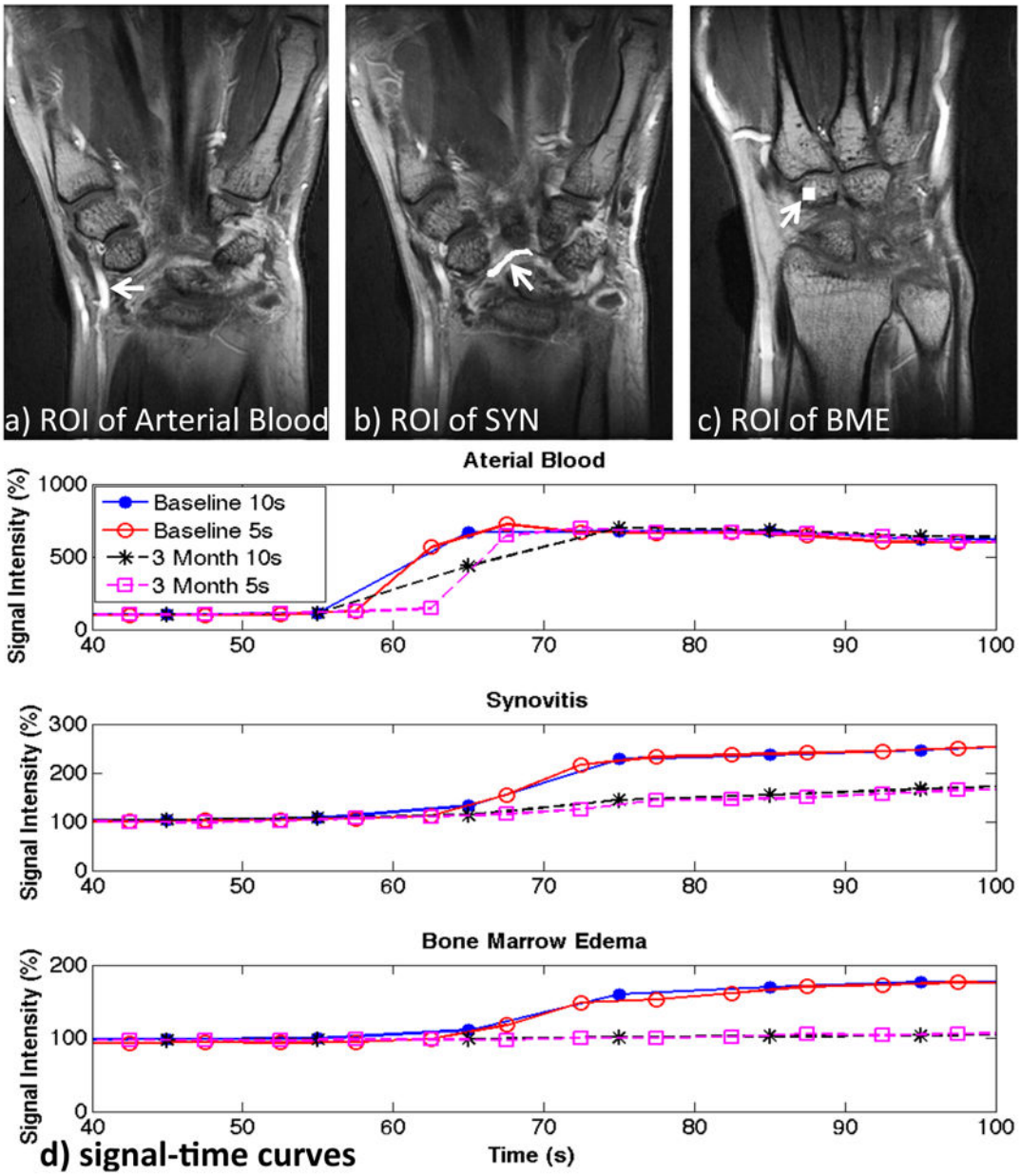

Figure 6.

Selected ROIs and its signal-to-time curves. **a-c)** show the selected ROIs of arterial blood, SYN and BME from the same patient in Figure 5. The corresponding signal-time curves at baseline and 3-month follow-up with the temporal resolution of 10s as well as 5s are shown in **d)**. Slower and lower contrast enhancements of SYN and BME showed at 3-month follow-up compared to those at baseline. The higher temporal resolution (5s) provides a better capture of the signal change during contrast injection, especially in arterial blood.

Table 1

RA-Patient clinical disease activity scores. Averaged scores and their standard deviations at baseline and 3-month follow-up visits are reported, as well as the changes in between two visits (n=10). Significant changes ($p<0.05$) are highlighted in bold and marked with *.

Patient clinical disease activity scores	Baseline	3-month follow-up	Change between baseline and 3-month follow-up
TEN28	7.5 ± 5.5	1.9 ± 2.9	**-5.6 ± 5.6***
SW28	10.5 ± 6.5	4.8 ± 3.7	**-5.7 ± 5 .0***
ESR (mm/hr)	38.1±22.9	37.1±18.6	-1.0 ± 14.7
CRP (mg/L)	18.2±25.6	10.1±9.4	-8.1 ± 19.8
DAS28-ESR	5.3 ± 1.8	3.9 ± 0.9	**-1.4 ± 1.6***
DAS28-CRP	4.7 ± 1.8	3.4 ± 1.0	-1.2 ± 1.5

Table 2

Perfusion parameters of a) synovitis and b) bone marrow edema, derived from DCE images of 10 s and 5 s temporal resolutions. Averaged measurements and their standard deviations are reported. Clinical SYN grading is listed in a).

a) SYN Perfusion parameters	**Baseline n=9**		**3-month follow-up n=8**		**Change between baseline and 3-month n=8**	
	10 s	**5 s**	**10 s**	**5 s**	**10 s**	**5 s**
dT (S)	112.8±52.1	125.9±63.7	124.3±50.7	137.5±59.9	10.7±39.4	7.9±53.0
MaxI (%)	219.6±79.0	223.3±81.4	218.1±83.2	218.4±82.2	-6.6±34.0	-10.7±34.0
TTP (s)	364.4±41.0	362.2±68.8	368.8±52.2	361.2±54.9	7.5±48.4	-0.6±47.7
Slope (%/min)	60.8±64.2	60.2±64.1	58.1±69.7	52.7±62.9	-6.8±61.0	-11.2±52.4
AUC (%hour)	20.3±6.8	20.4±6.9	20.1±7.4	19.9±7.2	-0.6±3.2	-1.0±3.3
AUCP (%hour)	17.7±4.6	17.8±5.0	17.6±5.3	17.1±5.2	-0.2±4.2	-1.0±4.4
SYN Grading	3.9±2.1		3.5±2.7		-0.4±1.3	
b) BME Perfusion parameters	Baseline n=9		3-month follow-up n=8		Change between baseline and 3-month n=8	
	10 s	5 s	10 s	5 s	10 s	5 s
dT (S)	89.4±56.2	104.1±57.1	84.1±63.6	137.1±84.5	6.0±71.4	36.0±70.8
MaxI (%)	168.9±49.3	172.0±49.0	163.7±52.8	166.8±52.9	-11.8±42.6	-11.4±40.4
TTP (s)	290.0±88.6	265.6±175.5	273.8±121.3	313.1±76.9	-8.8±175.7	38.8±97.1
Slope (%/min)	56.0±61.3	44.5±45.5	48.0±53.7	39.4±43.5	-14.6±23.3	-9.7±10.9
AUC (%hour)	16.4±4.0	16.5±4.0	15.9±4.5	15.9±4.3	-1.0±3.1	-1.0±2.9
AUCP (%hour)	11.5±4.5	10.5±4.3	11.3±6.4	12.4±5.5	-0.3±8.1	1.3±6.5

Table 3

Correlations between the perfusion parameters of SYN and the clinical disease activity scores at baseline. The correlation coefficients (highlighted as bold and marked with *) denote significant correlations ($p<0.05$). Clinical SYN grading is also listed for comparison.

SYN Perfusion parameters (baseline, n=9)	dT (S)		MaxI (%)		TTP (s)		Slope (%/min)		AUC (%hour)		AUCP (%hour)		SYN grading
Temporal resolution	**10 s**	**5 s**	**10 s**	**5 s**	**10 s**	**5 s**	**10 s**	**5 s**	**10 s**	**5 s**	**10 s**	**5 s**	
TEN28	**-0.85***	**-0.95***	**0.77***	**0.76***	-0.63	**-0.74***	**0.88***	**0.88***	**0.80***	**0.80***	0.63	0.60	0.62
SW28	-0.59	**-0.77***	**0.67***	**0.67***	-0.40	-0.34	0.57	0.60	**0.68***	**0.69***	0.59	0.66	**0.80***
ESR	0.49	0.28	0.03	0.04	0.26	0.49	-0.08	-0.10	-0.00	0.00	0.07	0.16	0.28
CRP	-0.52	-0.54	0.56	0.57	-0.33	-0.21	0.46	0.47	0.56	0.57	0.50	0.57	0.42
DAS28-ESR	-0.53	**-0.80***	**0.69***	**0.67***	-0.25	-0.26	0.60	0.61	**0.68***	**0.68***	**0.67***	0.66	**0.75***
DAS28-CRP	**-0.70***	**-0.87***	**0.69***	**0.68***	-0.35	-0.38	0.62	0.65	**0.70***	**0.69***	0.66	0.64	0.63
SYN grading	-0.30	-0.56	**0.71***	**0.71***	-0.26	-0.19	0.57	0.58	**0.71***	**0.72***	**0.69***	**0.73***	

Table 4

Correlations between the changes of the perfusion parameters of SYN and the changes of the clinical disease activity scores over a 3-months follow-up time. The highlighted numbers (bold and marked with *) denote significant correlations ($p<0.05$).

SYN Perfusion parameters (baseline, n=8)	dT (S)		MaxI (%)		TTP (s)		Slope (%/min)		AUC (%hour)		AUCP (%hour)		SYN grading
Temporal resolution	**10 s**	**5 s**	**10 s**	**5 s**	**10 s**	**5 s**	**10 s**	**5 s**	**10 s**	**5 s**	**10 s**	**5 s**	
TEN28	-0.64	-0.65	**0.74***	**0.83***	-0.33	-0.16	**0.73***	**0.75***	**0.77***	**0.83***	0.22	0.43	0.49
SW28	-0.22	-0.35	0.47	0.53	0.27	0.43	0.11	0.13	0.38	0.42	0.54	**0.74***	-0.19
ESR	0.08	-0.18	-0.11	-0.01	0.16	0.35	-0.10	-0.07	-0.12	-0.04	0.06	0.34	-0.27
CRP	-0.60	-0.53	0.16	0.22	-0.26	-0.15	0.30	0.34	0.18	0.21	-0.11	0.02	0.06
DAS28-ESR	-0.50	**-0.79***	0.53	0.60	-0.06	-0.11	0.43	0.47	0.51	0.55	0.24	0.34	0.20
DAS28-CRP	-0.63	**-0.82***	0.60	0.68	-0.21	-0.18	0.56	0.60	0.60	0.66	0.20	0.35	0.33
SYN grading	-0.60	-0.48	0.48	0.53	**-0.82***	**-0.81***	**0.92***	**0.93***	0.64	0.67	-0.36	-0.33	